

# Missing MRI Pulse Sequence Synthesis using Multi-Modal Generative Adversarial Network

Anmol Sharma, *Student Member, IEEE*, Ghassan Hamarneh, *Senior Member, IEEE*

**Abstract**—Magnetic resonance imaging (MRI) is being increasingly utilized to assess, diagnose, and plan treatment for a variety of diseases. The ability to visualize tissue in varied contrasts in the form of MR pulse sequences in a single scan provides valuable insights to physicians, as well as enabling automated systems performing downstream analysis. However many issues like prohibitive scan time, image corruption, different acquisition protocols, or allergies to certain contrast materials may hinder the process of acquiring multiple sequences for a patient. This poses challenges to both physicians and automated systems since complementary information provided by the missing sequences is lost. In this paper, we propose a variant of generative adversarial network (GAN) capable of leveraging redundant information contained within multiple available sequences in order to generate one or more missing sequences for a patient scan. The proposed network is designed as a multi-input, multi-output network which combines information from all the available pulse sequences, implicitly infers which sequences are missing, and synthesizes the missing ones in a single forward pass. We demonstrate and validate our method on two brain MRI datasets each with four sequences, and show the applicability of the proposed method in simultaneously synthesizing all missing sequences in any possible scenario where either one, two, or three of the four sequences may be missing. We compare our approach with competing unimodal and multi-modal methods, and show that we outperform both quantitatively and qualitatively.

**Index Terms**—generative adversarial networks, multi-modal, missing modality, pulse sequences, MRI, synthesis.

## I. INTRODUCTION

**M**EDICAL imaging forms the backbone of the modern healthcare systems, providing means to assess, diagnose, and plan treatments for a variety of diseases. Imaging techniques like computed tomography (CT), magnetic resonance imaging (MRI), X-Rays have been in use for over many decades. Magnetic resonance imaging (MRI) out of these is particularly interesting in the sense that a single MRI scan is a grouping of multiple pulse sequences, each of which provides varying tissue contrast views and spatial resolutions, without the use of radiation. These sequences are acquired by varying the spin echo and repetition times during scanning, and are widely used to show pathological changes in internal organs and musculoskeletal system. Some of the commonly acquired sequences are  $T_1$ -weighted,  $T_2$ -weighted,  $T_1$ -with-contrast-enhanced ( $T_{1c}$ ), and  $T_2$ -fluid-attenuated inversion recovery ( $T_{2flair}$ ), though there exist many more [1].

A combination of sequences provide both redundant and complimentary information to the physician about the imaged tissue, and certain diagnosis are best performed when a

particular sequence is observed. For example,  $T_1$  and  $T_{2flair}$  sequences provide clear delineations of the edema region of tumor in case of glioblastoma,  $T_{1c}$  provides clear demarcation of enhancing region around the tumor used as an indicator to assess growth/shrinkage, and  $T_{2flair}$  sequence is used to detect white matter hyperintensities for diagnosing vascular dementia (VD) [2].

In clinical settings, however, it is common to have MRI scans acquired using varying protocols, and hence varying sets of sequences per patient. Sequences which are routinely acquired may be unusable or missing altogether due to scan corruption, artifacts, incorrect machine settings, allergies to certain contrast agents and limited available scan time [3]–[5]. This phenomenon is problematic for many downstream data analysis pipelines that assume presence of a certain set of pulse sequences to perform their task. For instance, most of the segmentation methods [6]–[10] proposed for brain MRI scans depend implicitly on the availability of a certain set of sequences in their input in order to perform the task. Most of these methods are not designed to handle missing inputs, and hence may fail in the event where some or most of the sequences may be absent.

Modifying existing pipelines in order to handle missing sequences is hard, and may lead to performance degradation. Also, the option of redoing a scan to acquire the missing/corrupted sequence is impractical due to the expensive nature of the acquisition, longer wait times for patients with non-life-threatening cases, need for registration between old and new scans, and rapid changes in anatomy of area in-between scan times due to highly active abnormalities such as glioblastoma. Hence there is a clear advantage in retrieving any missing sequence or an estimate thereof, without having to redo the scan or changing the downstream pipelines.

To this end, we propose a multi-modal generative adversarial network (MM-GAN) which is capable of synthesizing missing sequences by combining information from all available sequences. The proposed method exhibits the ability to synthesize, with high accuracy, all the required sequences which are deemed missing in a single forward pass through the network. The term “multi-modal” simply refers to the fact that the GAN can take multiple-modalities of available information as input, which in this case represents different pulse sequences. Similar to the input being multi-modal, our method generates multi-modal output containing synthesized versions of the missing sequences. Since most of the downstream analysis pipelines commonly target  $M = 4$  pulse sequences  $S = \{T_1, T_{1c}, T_2, T_{2flair}\}$  as their input [7], [11], [12], we design our method around the same number of sequences, although we note that our method can be generalized to any number  $M$

Anmol Sharma and Ghassan Hamarneh are with the Medical Image Analysis Laboratory, School of Computing Science, Simon Fraser University, Canada. e-mail: {asa224, hamarneh}@sfu.ca

and set  $S$  of sequences. The input to our network is a 4-channel (corresponding to  $M = 4$  sequences) 2D axial slice, where random Gaussian noise is imputed for channels corresponding to missing sequences. The output of the network is a 4-channel 2D axial slice, in which the originally missing sequences are synthesized by the network.

The rest of the paper is organized as follows: Section II presents a review of the MR sequence synthesis literature. Section IV presents the proposed method in detail. Section III provides an overview of the key contributions of this work. Section V provides details about the method implementation, datasets used, as well as outlines experimental setup for the current work. Section VI discusses the results and observations for the proposed method, and finally the paper is concluded in Section VII.

## II. RELATED WORK

There has been an increased amount of interest in developing methods for synthesizing MR pulse sequences [2], [5], [13]–[26]. We present a brief overview of previous work in this field by covering them in two sections: Unimodal, where both the input and output of the system is a single pulse sequence; and multimodal, where methods are able to leverage multiple input sequences to synthesize a single or multiple sequences.

### A. Unimodal Synthesis

In unimodal synthesis, a common strategy includes building an atlas or a database that maps intensity values between given sequences. Jog et al. [15] used a bagged ensemble of regression trees trained from an atlas. The training data  $(\mathcal{A}_1, \mathcal{A}_2)$  consisted of multiple image patches  $\mathcal{A}_1$  around a voxel  $i$  in a source sequence, and a single intensity value at the same voxel in a target sequence, as  $\mathcal{A}_2$ . The use of image patches to predict the intensity value of a single voxel in output sequence allows representing many-to-many relationship between intensity values of input and target sequences. Ye et al. [14] propose an inverse method, which performs a local patch-based search in a database for every voxel in the target pulse sequence. Once the patches are found, they are “fused” together using a data-driven regularization approach. Another atlas based method was proposed in [19] where  $T_2$  whole-head sequence (including skull, eyes etc.) is synthesized from the available  $T_1$  images. The synthesized  $T_2$  sequence is used to correct distortion in diffusion-weighted MR images by using it as template for registration, in the absence of a real  $T_2$  sequence. Yawen et al. [20] leverage joint dictionary learning (JDL) for synthesizing any unavailable MRI sequence from available MRI data. JDL is performed by minimizing the inconsistency between statistical distributions of the dictionary codes for input MRI sequences while preserving the geometrical structure of the input image.

Supervised machine learning and deep learning (DL) based methods have also been employed in sequence synthesis pipelines. A 3D continuous-valued conditional random field (CRF) is proposed in [18] to synthesize  $T_2$  images from  $T_1$ . The synthesis step is encoded as a maximum a-posterior (MAP) estimate of Gaussian distribution parameters built from

a learnt regression tree. Nguyen et al. [27] was one of the first to employ DL in the form of location-sensitive deep network (LSDN) for sequence synthesis. LSDN predicts the intensity value of the target voxel by using voxel-centered patches extracted from an input sequence. The network models the responses of hidden nodes as a product of feature and spatial responses. Similarly, Bowles et al. [2] generate “pseudo-healthy” images by performing voxel-wise kernel regression instead of deep networks to learn local relationships between intensities in  $T_1$  and  $T_{2flair}$  sequences of healthy subjects. Since most of the methods were based on local features in the form of patches and did not leverage global features of the input sequence, Sevettidis et al. [21] proposed an encoder-decoder style deep neural network trained layer-wise using restricted Boltzmann machine (RBM) based training. The method utilized global context of the input sequence by taking a full slice as input. Recently, Jog et al. [22] propose a random forest based method that learns intensity mapping between input patches centered around a voxel extracted from a single pulse sequence, and the intensity of corresponding voxel in target sequence. The method utilized multi-resolution patches by building a Gaussian pyramid of the input sequence. Yu et al. [26] propose a unimodal GAN architecture to synthesize missing pulse sequences in a one-to-one setting. The approach uses an edge detection module that tries to preserve the high-frequency edge features of the input sequence, in the synthesized sequence. Recently, Ul Hassan Dar et al. [28] propose to use a conditional GAN to synthesize missing MR pulse sequences in a unimodal setting for two sequences  $T_1$  and  $T_2$ .

### B. Multimodal Synthesis

Multimodal synthesis has been a relatively new and unexplored avenue in MR synthesis literature. One of the first multi-input, single-output method was proposed by Jog et al. [16]; a regression based approach to reconstruct  $T_{2flair}$  sequence using combined information from  $T_1$ ,  $T_2$ , and proton density (PD) sequences. Reconstruction is performed by a bagged ensemble of regression trees predicting the  $T_{2flair}$  voxel intensities. Chartsias et al. [5] were one of the first to propose a multi-input, multi-output encoder-decoder based architecture to perform many-to-many sequence synthesis, although their method is tested only using a single-output ( $T_{2flair}$ ). Their network is trained using a combination of three loss functions, and uses a feature fusion step in the middle that separates the encoders and decoders. Olut et al. [23] present a GAN based framework to generate magnetic resonance angiography (MRA) sequence from available  $T_1$ , and  $T_2$  sequences. The method uses a novel loss function formulation, which preserves and reproduces vascularities in the generated images. Although for a different application, Mehta et al. [24] proposed a multi-task, multi-input, multi-output 3D CNN that outputs a segmentation mask of the tumor, as well as a synthesized version of  $T_{2flair}$  sequence. The main aim remains to predict tumor segmentation mask from three available sequences  $T_1$ ,  $T_2$ , and  $T_{1c}$ , and no quantitative results for  $T_{2flair}$  synthesis using  $T_1$ ,  $T_2$ , and  $T_{1c}$  are provided.

Though all the methods discussed above propose a multi-input method, none of the methods have been proposed to synthesize multiple missing sequences (multi-output), and in one single pass. All three methods [16], [5], and [24] synthesize only  $T_{2flair}$  sequence in the presence of varying number of input sequences, while [23] only synthesizes MRA using information from multiple inputs. Although the work presented in [23] is close to our proposed method, theirs is not a truly multimodal network, since there is no empirical evidence that their method will generalize to multiple scenarios. To the best of our knowledge, we are the first to propose a method that is capable of synthesizing multiple missing sequences using a combination of various input sequences, and demonstrate the method on the complete set of scenarios (i.e., all combinations of missing sequences).

The main motivation for most synthesis methods is to retain the ability to meaningfully use some downstream analysis pipelines like segmentation or classification despite the partially missing input. However, there have been efforts by researchers working on those analysis pipelines to bypass any synthesis step by making the analysis methods themselves robust to missing sequences. Most notably, Havai et al. [3] and Varsavsky et al. [4] provide methods for tumor segmentation using brain MRI that are robust to missing sequences [3], or to missing sequence labels [4]. Although the methods bypass the requirement of having a synthesis step before actual downstream analysis, the performance of these robust versions of analysis pipelines often do not match the state-of-the-art performance of other non-robust methods in the case when all sequences are present. This is due to the fact that the methods not only have to learn how to perform the task (segmentation/classification) well, but also to handle any missing input data. This two-fold objective for a single network raises a trade-off between robustness and performance.

### III. CONTRIBUTIONS

The following are the key contributions of this work:

- 1) We propose the first MR pulse sequence synthesizer capable of synthesizing missing pulse sequences using *any combination of available sequences as input* without the need for tuning or retraining of models.
- 2) The proposed method is capable of synthesizing *any combination of target missing sequences as output* in one single forward pass, which essentially eliminates the need to perform multiple runs in order to generate more than one missing sequence.
- 3) We demonstrate that the proposed method does not need explicit supervision or conditioning in order to synthesize a particular missing sequence. Instead, the proposed method relies on a combination of three design choices for implicit conditioning, namely imputed noise in the input in place of missing sequences, sequence-selective loss computation in the generator, and sequence-selective discrimination.
- 4) To the best of our knowledge, we are the first to incorporate curriculum learning based training for GAN

by varying the difficulty of examples shown to the network during training.

- 5) Through experiments, we show that we outperform both the current state-of-art in unimodal [22], [28], as well as multi-modal missing pulse sequence synthesis [5] methods. We also set up new benchmarks on a complete set of scenarios using the BraTS2018 dataset.

## IV. METHODOLOGY

### A. Background

Generative adversarial networks (GANs) were first proposed by Goodfellow et al. [29] in order to generate realistic looking images. A GAN is typically built using a combination of two networks: generator ( $\mathcal{G}$ ) and discriminator ( $\mathcal{D}$ ). The generator network is tasked with generating realistic data, typically by learning a mapping from a random vector  $z$  to an image  $I$ ,  $\mathcal{G} : z \rightarrow I$ , where  $I$  is said to belong to the generator's distribution  $p_{\mathcal{G}}$ . The discriminator  $\mathcal{D} : I \rightarrow t$  maps its input  $I$  to a target label  $t \in \{0, 1\}$ , where  $t = 0$  if  $I \in p_{\mathcal{G}}$ , i.e. a fake image generated by  $\mathcal{G}$  and  $t = 1$  if  $I \in p_r$  where  $p_r$  is the distribution of real images. A variant of GANs, called conditional-GAN (cGAN) [30], proposes a generator that learns a mapping from a random vector  $z$  and a class label  $y$  to an output image  $I \in p_{\mathcal{G}}$ ,  $\mathcal{G} : (z, y) \rightarrow I$ . Another variant of cGAN called Pix2Pix [31] develops a GAN in which the generator learns a mapping from an input image  $x \in p_r$  to output image  $I \in p_{\mathcal{G}}$ ,  $\mathcal{G} : x \rightarrow I$ , and the discriminator learns a mapping from two input images,  $x_1$  and  $x_2$ , to  $T$ ,  $\mathcal{D} : (x_1, x_2) \rightarrow T$ .  $x_1$  and  $x_2$  may belong to either  $p_r$  (real) or  $p_{\mathcal{G}}$  (fake). The output  $T$  in this case is not a single class label, but a binary prediction tensor representing whether each  $N \times N$  patch in the input image is real or fake [31].

A GAN is trained in an adversarial setting, where the generator (parameterized by  $\theta_{\mathcal{G}}$ ) is trained to synthesize realistic output that can "fool" the discriminator into classifying them as real, and the discriminator (parameterized by  $\theta_{\mathcal{D}}$ ) is trained to accurately distinguish between real data and fake data synthesized by the generator. GAN input/outputs can be images [31], text [32] or even music [33]. Both the generator and discriminator act as adversaries to each other, hence the training formulation forces both networks to continuously get better at their tasks. GANs found tremendous success in a variety of different tasks, ranging from face-image synthesis [34], image stylization [35], future frame prediction in videos [36], text-to-image synthesis [32] and synthesize scene images using scene attributes and semantic layout [37]. GANs have also been utilized in medical image analysis [38], particularly for image segmentation [39]–[41], normalization [42], synthesis [23], [26], [28] as well as image registration [43].

### B. Proposed Method

We propose a variant of Pix2Pix architecture [31] called Multi-Modal Generative Adversarial Network (MM-GAN) for the task of synthesizing missing MR pulse sequences in a single forward pass while leveraging all available sequences. The following subsections would outline the detailed architecture of our model.

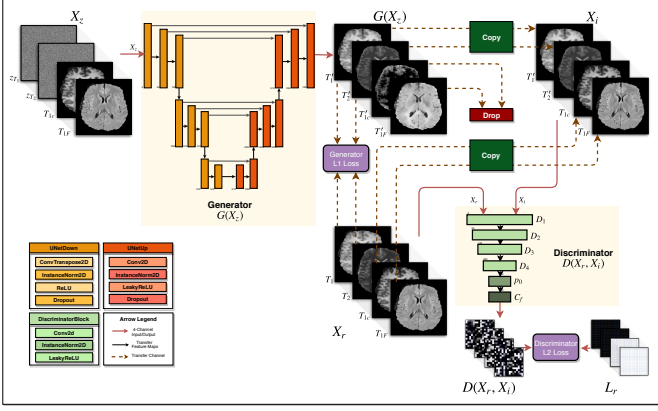


Fig. 1. Proposed multimodal generative adversarial network (MM-GAN) training process. Best viewed electronically.

1) *Generator*: The generator of the proposed method is a UNet [44], which has proven useful in a variety of segmentation and synthesis tasks due to its contracting and expanding paths in the form of encoder and decoder subnetworks. The architecture is illustrated in Figure 1. The convolution kernel sizes for each layer in the generator is set to  $4 \times 4$ . The generator network is a combination of UNetUp and UNetDown blocks. The input to the generator is a 2D axial slice from a patient scan with  $C = 4$  channels representing four pulse sequences, and spatial size of  $256 \times 256$  pixels. The network is designed with a fixed input size of 4-channels, where channel  $C = 0, 1, 2$ , and  $3$  corresponds to  $T_1$ ,  $T_2$ ,  $T_{1c}$ , and  $T_{2flair}$ , respectively. In order to synthesize missing sequences, the channels corresponding to each missing sequence are imputed with random noise sampled from the normal distribution  $\mathcal{N}(0, 1)$ . The imputed version (along with the real sequences) becomes the input to the generator and is represented by  $X_z$ . For instance, if sequences  $T_1$  and  $T_2$  are missing, channels  $C = 0$  and  $C = 1$  in the input image are imputed with random noise image of size  $256 \times 256$ . The output of the generator is given by  $\mathcal{G}(X_z|\theta_G)$  and is of the same size as the input. Due to design, the generator always outputs 4-channels, however, as we outline in the subsequent text the output channels corresponding to the existing real sequences are not used for loss computation and are replaced with the real sequences before relaying them as input to the discriminator. During training the ground truth image  $X_r$ , short for “real”, which is of the same size as  $X_z$  contains all ground truth sequences at their respective channel indices. We use the term “image” for a single 2D slice with 4 channels.

MM-GAN observes both an input image and random noise in the form of  $X_z$ , in contrast to vanilla Pix2Pix where the generator does not observe any random noise and is conditioned just by an observed image  $x$ . The reasons behind this design choice are discussed in subsection IV-B3.

To optimize  $\theta_G$ , our generator adopts the general form of the generator loss in Pix2Pix, which is a combination of a reconstruction loss  $\mathcal{L}_1$  and an adversarial loss  $\mathcal{L}_2$  used to train the generator to fool the discriminator, i.e.

$$\theta_G^* = \arg \min_{\theta_G} \lambda \mathcal{L}_1(\mathcal{G}(X_z|\theta_G), X_r) + (1 - \lambda) \mathcal{L}_2(\mathcal{D}(X_i, X_r|\theta_D), L_{ar}). \quad (1)$$

To calculate  $\mathcal{L}_1$ , we select synthesized sequences from  $\mathcal{G}(X_z|\theta_G)$ , that were originally missing, and compute the L1 norm of the difference between the synthesized versions of the sequence and the available ground truth from  $X_r$ . Mathematically, given the set  $K$  containing the indices of missing sequences (e.g.  $K = \{0, 2\}$  when  $T_1$  and  $T_{1c}$  are missing) in the current input, we calculate  $\mathcal{L}_1$  only for the sequences that are missing ( $k = 0, 2$ ), and sum the values.

To calculate  $\mathcal{L}_2$ , we compute the squared L2 norm of the difference between the discriminator’s predictions  $\mathcal{D}(X_i, X_r|\theta_D)$  and a dummy ground truth tensor  $L_{ar}$  of the same size as the output of  $\mathcal{D}$ . In order to encourage the generator to synthesize sequences that confuse or “fool” the discriminator into predicting they are real, we set all entries of  $L_{ar}$  to ones, masquerading all generated sequences as real.  $X_i$  is introduced in the next section.

The choice of L1 as a reconstruction loss term for the generator is motivated by its ability to prevent too much blurring in the final synthesized sequences, as compared to using an L2 loss (similar to [31]).

2) *Discriminator*: We use the PatchGAN architecture [31] for the discriminator part of our MM-GAN. PatchGAN architecture learns to take into account the local characteristics of its input, by predicting a real/fake class for every  $N \times N$  patch of its input, compared to classic GANs where the discriminator outputs a single real/fake prediction for the whole input image. This encourages the generator to synthesize images not just with proper global features (shape, size), but also with accurate local features (texture, distribution, high-frequency details). In our case we set  $N = 16$ .

The discriminator is built using four blocks followed by a zero padding layer and a final convolutional layer (Figure 1). The convolutional kernel sizes, stride and padding is identical to the values used in the generator (subsection IV-B2). Due to the possibility of having a varying number of sequences missing, instead of providing just the synthesized sequences and their real counterparts as input to the discriminator, we first create a modified version of  $\mathcal{G}(X_z|\theta_G)$  by dropping the synthesized sequences that were originally present, and replacing them with the original sequences from  $X_r$ . The modified version of  $\mathcal{G}(X_z|\theta_G)$  is represented by  $X_i$ , short for “imputed”. The input to the discriminator is a concatenation of  $X_i$  and  $X_r$ . This is also illustrated in Figure 1.

The discriminator is trained to output a 2D patch of size  $16 \times 16$  pixels, with 4 channels corresponding to each sequence. In order to supervise the discriminator during training, we use a 4-channel 2D image based target, in which each channel corresponds to a sequence. More specifically, given missing sequences  $K$  (e.g.,  $K = \{0, 2\}$ ,  $T_1$  and  $T_{1c}$  missing), the target (i.e. ground truth) variable for  $\mathcal{D}$  is  $L_r^k = \{0.0 \text{ (fake) if } k \in K, \text{ else } 1.0 \text{ (real)}\}$ . Note that  $L_r^k$  is a 2D tensor of size  $16 \times 16$  (since each  $256 \times 256$  image is divided into  $16 \times 16$  patches) yet the assignment of 0.0 or 1.0 represents an assignment to the

whole  $16 \times 16 \times L_r^k$  tensor (since the whole image is either real or fake and not patch-specific). This is also illustrated in Figure 1.

Between the output of discriminator  $\mathcal{D}(X_i, X_r | \theta_D)$  and  $L_r$ , an L2 loss is computed. The final discriminator loss becomes:

$$\theta_D^* = \arg \min_{\theta_D} \mathcal{L}_2(\mathcal{D}(X_r, X_r | \theta_D), L_{ar}) + \mathcal{L}_2(\mathcal{D}(X_r, X_i | \theta_D), L_r). \quad (2)$$

3) *Implicit conditioning*: In order to make the generator generalize to all possible scenarios where one or more sequences may be missing, it is imperative that the generator has the ability to recognize which sequence is actually missing, and which ones are present. Previously, approaches like the cGAN [30] explicitly condition the generator as a “supervision” to generate an image of a particular class. However, in this work, we note that this may not be necessary, and the conditioning can be performed implicitly using a combination of three design choices: noise imputation in place of missing sequences for input to  $\mathcal{G}$ ; selective loss computation in  $\mathcal{G}$ ; and selective discrimination in  $\mathcal{D}$ .

**NOISE IMPUTATION**: The input  $X_z$  of the generator always contains random noise in place of the missing sequences which acts as a way to condition the generator and informs which sequence(s) to synthesize.

**SELECTIVE LOSS COMPUTATION IN  $\mathcal{G}$** : In conjunction, the  $\mathcal{L}_1(\mathcal{G})$  loss that is computed only between the synthesized sequences for the generator, and then backpropagated, allows the generator to align itself towards only synthesizing the actual missing sequences properly while ignoring the performance in synthesizing the ones that were already present.

**SELECTIVE DISCRIMINATION IN  $\mathcal{D}$** : Imputing real sequences at the generator output (i.e.  $X_i$ ) before providing it as discriminator input forces the discriminator to accurately learn to delineate only between the synthesized sequences and their real counterparts. Since the generator loss function also has a term that tries to fool the discriminator, this allows selective backpropagation into the generator where it is penalized only for incorrectly synthesizing the missing sequences, and not for incorrectly synthesizing the sequences that were already present. This also relieves the generator of the difficult task of synthesizing all sequences in the presence of some sequences.

4) *Curriculum learning*: In order to train our proposed method we use a curriculum learning (CL) [45] based approach. In CL based training, the network is initially shown easier examples followed by increasingly difficult examples as the training progresses. In our case, the difficulty of examples increases as more sequences go missing. Initially, the network is shown scenarios with only one missing sequence. As the training progresses, scenarios with two or more sequences missing are sampled for training. After a certain threshold epoch as the training nears the end, all scenarios are made equally likely to be shown to the network during training.

## V. EXPERIMENTAL SETUP

In this section we describe different aspects of the experiments that are performed in this work.

### A. Datasets

In order to validate our method we use brain MRI datasets from two sources, namely the Ischemic Stroke Lesion Segmentation Challenge 2015 (ISLES2015) and the Multimodal Brain Tumor Segmentation Challenge 2018 (BraTS2018).

1) *ISLES2015* dataset is a publicly available database with multi-spectral MR images. We choose the sub-acute ischemic stroke lesion segmentation (SISS) cohort of patients, which contains 28 training and 36 testing cases. The patient scans are skull stripped, and resampled to an isotropic resolution of  $1 \text{ mm}^3$ . Each scan consists of four sequences namely  $T_1$ ,  $T_2$ , DWI, and  $T_{2\text{flair}}$ , and are co-registered to the  $T_{2\text{flair}}$  sequence. We use 22 patients from the SISS training set for experiments.

2) *BraTS2018* consists of a total of 285 patient MR scans acquired from 19 different institutions, divided into two cohorts: glioblastoma (GBM/HGG) and lower grade glioma (LGG). The patient scans contains four pulse sequence  $T_1$ ,  $T_2$ ,  $T_{1c}$ , and  $T_{2\text{flair}}$ . All scans are resampled to  $1 \text{ mm}^3$  isotropic resolution, skull stripped, and co-registered with a single anatomical template. In order to demonstrate our method’s ability in synthesizing sequences with both high grade and low grade glioma tumors present, we use a total of 210 patients from HGG and 75 from LGG cohort. 195 patients are reserved for training for HGG cohort, while 65 are used for training in LGG experiments. For validation, we use 5 patients for both HGG and LGG cohorts. In order to test our trained models, we use 10 patients from HGG cohort (due to larger data available), while we report results using 5 patients for LGG cohort as testing.

### B. Preprocessing

Each patient scan is normalized by dividing each sequence by its mean intensity value. This ensures that distribution of intensity values is preserved. In order to crop out the brain region from each sequence, we calculate the largest bounding box that can accommodate each brain in the whole dataset, and then use the coordinates to crop each sequence in every patient scan. The final cropped size of a single patient scan with all sequences contains 148 axial slices of size  $194 \times 155$ . Each slice in every sequence is resized to a spatial resolution of  $256 \times 256$ , using bilinear interpolation, in order to maintain compatibility with UNet architecture of the generator.

### C. Benchmark Methods

We compare our method with three competing methods, one unimodal and two multimodal. The unimodal (single-input, single-output) method we compare against is pGAN [28], while the multimodal (multi-input, single-output) models being REPLICIA [22], and that of Chartsias et al. [5], called MM-Synthesis hereafter. For comparison with pGAN [28], we reimplement the method using the same open-source framework used in the original paper, and train both pGAN and our method on a randomly chosen subset of data from BraTS2018 LGG cohort. For our multimodal experiments, we recreate the

exact same testbed as in MM-Synthesis, using the same testing strategy (5-fold cross validation), database (ISLES2015), and scenarios (7 scenarios where  $T_{2flair}$  is always missing and is the only one that is synthesized). Since MM-Synthesis reimplements REPLICa, we report mean squared error (MSE) results for both REPLICa and MM-Synthesis from [5]. For our extended set of experiments, we perform testing on the HGG and LGG cohorts of BRaTS2018 dataset for which we report results of all 14 valid scenarios (=16-2, as scenario when all sequences are missing/present are invalid for our experiments) instead of just 7, which showcases our method’s generalizability on different use-cases and difficulty levels.

#### D. Training and Implementation Details

In order to optimize our networks, we use Adam [46] optimizer with learning rate  $\eta = 0.0002$ ,  $\beta_1 = 0.5$  and  $\beta_2 = 0.999$ . Both the generator and discriminator networks are initialized with weights sampled from a Gaussian distribution with  $\mu = 0$ ,  $\sigma = 0.02$ . We perform three experiments, first for establishing that multi-input synthesis is better than single-input, second for  $T_{2flair}$  synthesis (multi-input, single output) using ISLES2015 dataset to compare with REPLICa and MM-Synthesis, and third multimodal synthesis (multi-input, multi-output) to set a new benchmark using BraTS2018 dataset. We refer to latter two experiments as MISO and MIMO, respectively, hereafter. We use a batch size of 4 slices to train models, except for MISO, where we use batch size of 2. We train the models for 60 epochs in both MISO and MIMO sets of experiments, with no data augmentation. Both the generator and discriminator networks are initialized with weights sampled from Gaussian distribution with  $\mu = 0$ ,  $\sigma = 0.02$ .

We choose  $\lambda = 0.9$  for the generator loss given in equation 1, while we multiply the discriminator loss by 0.5 which essentially slows down the rate at which discriminator learns compared to generator. During each epoch, we alternate between a single gradient descent step on the generator, and one single step on the discriminator.

For our MIMO experiments, we use the original PatchGAN [31] discriminator. However for our MISO experiments, due to lack of training data, we used a smaller version of the PatchGAN discriminator with just two discriminator blocks, followed by a zero padding and final convolution layer. Also, random noise was added to both  $X_r$  and  $X_i$  inputs of the discriminator in MISO experiments. This was done to reduce the complexity of the discriminator to prevent it from overpowering the generator, which we observed when original PatchGAN with no noise imputation in its inputs was used for this set of experiments. The generator’s final activation was set to ReLU for MIMO and linear for MISO experiments due to the latter having negative intensity values for some patients.

For our implementation we used Python as our main programming language. We implemented Pix2Pix architecture in PyTorch. The computing hardware consisted of an i7 CPU with 64 GB RAM and GTX1080Ti 12 GB VRAM GPU. Throughout our experiments we use random seeding in order to ensure reproducibility of our experiments. For our MIMO experiments, we use curriculum learning by raising

the difficulty of scenarios every 10 epochs (starting from one missing sequence) that are shown to the network until epoch 30 (shown examples with three missing sequences), after which the scenarios are shown randomly with uniform probability until epoch 60. For MISO experiments we train the model without curriculum learning, and show all scenarios with uniform probability to the network for 30 epochs. MM-GAN takes an average time of  $0.1536 \pm 0.0070$  seconds per patient as it works in constant time at test-time w.r.t number of sequences missing.

#### E. Evaluation Metrics

Evaluating the quality of synthesized images should ideally take into account both the quantitative aspect (per pixel synthesis error) as well as qualitative differences mimicking human perception. In order to cover this spectrum, we report results using three metrics, namely mean squared error (MSE), peak signal-to-noise ratio (PSNR) and structural similarity index metric (SSIM). The MSE is given as  $\frac{1}{n} \sum_{i=1}^N (y_i - y'_i)^2$  where  $y_i$  is the original sequence and  $y'_i$  is the synthesized version. MSE however depends heavily on the scale of intensities, hence for fair comparison, similar intensity normalization procedures were followed. In this work, we adopt the normalization procedure used in [5], and report all results with the same normalization type. However in order to still provide a normalization agnostic metric, we report PSNR, which takes into account both the MSE and the largest possible intensity value of the image, given as:  $10 \log_{10} (I_{max}^2 / \text{MSE})$ , where  $I_{max}$  is the maximum intensity value that the image supports, which depends on the datatype. We also report SSIM, which tries to capture the human perceived quality of images by comparing two images. SSIM is given as:  $\frac{(2\mu_x\mu_y+c_1)(2\sigma_{xy}+c_2)}{(\mu_x^2+\mu_y^2+c_1)(\sigma_x^2+\sigma_y^2+c_2)}$ , where  $x, y$  are two images to be compared, and  $\mu$  = mean intensity,  $\sigma^2$  = variance of image, and  $\sigma_{xy}$  = covariance of  $x, y$ .

## VI. RESULTS AND DISCUSSION

In this section we present the results for our experiments validating our method and comparison with competing unimodal and multimodal methods.

#### A. Single-Input VS Multi-Input Synthesis

In order to understand the performance difference between using a single sequence versus using information from multiple sequences to synthesize a missing sequence, we set up an experiment comparing the two approaches. Our hypothesis for this experiment is that multiple sequences provide complementary information about the imaged tissue, and hence should be objectively better than just using one sequence. We set up an experiment to compare multi-input model with a single-input model to synthesize missing  $T_1$  and  $T_2$  sequences. We train two baseline models, which are the single-input versions of MM-GAN. We note that our choice of baseline model was first presented in its original form in [28] called pGAN. pGAN is a special case of our proposed MM-GAN where number of inputs = outputs = 1, and no noise tensor is explicitly observed

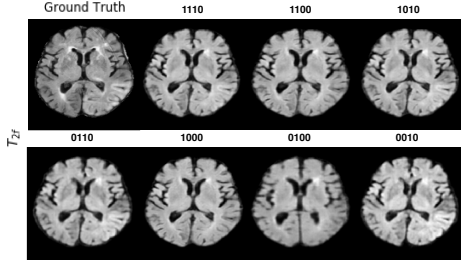


Fig. 2. Qualitative results from  $T_{2flair}$  synthesis experiments with ISLES2015 dataset. The order of scenario bit-string is  $T_1$ ,  $T_2$ , DW,  $T_{2flair}$ . Patient images shown here are from VSD ID 70668 from ISLES2015 SISS cohort.

by the generator. pGAN does not generalize to multiple sequences, or scenarios. We call the baseline models pGAN $_{T_1}$  (synthesizing  $T_1$  from  $T_2$ ) and pGAN $_{T_2}$  (synthesizing  $T_2$  from  $T_1$ ), and implement them as reported in the original paper [28]. For our multi-input version, we train two variants of the proposed MM-GAN, called MI-GAN (multi-input GAN). The two MI-GANs called MI-GAN $_{T_1}$  and MI-GAN $_{T_2}$  synthesize  $T_1$  from  $(T_2, T_{1c}, T_{2flair}, z)$  and  $T_2$  from  $(T_1, T_{1c}, T_{2flair}, z)$  respectively, where  $z$  = noise tensor of identical shape as a single sequence slice. Table I presents our results from our experiment where we train both pGAN and MI-GAN on 70 patients for 30 epochs from LGG cohort and test on 5 patients. We observe that synthesizing missing sequences using a combination of input sequences is consistently superior to using just one single sequence. We note that MM-GAN variants perform better than pGAN variants in all three metrics (MSE, PSNR and SSIM). This suggests that there is ample complimentary information available between sequences that can be leveraged by a GAN to synthesize a missing sequence.

TABLE I  
COMPARISON BETWEEN pGAN AND MI-GAN. VALUES IN BOLDFACE REPRESENT WINNING PERFORMANCE VALUES.

Model	MSE	PSNR	SSIM
pGAN $_{T_1}$	0.1191	24.1158	0.8895
MI-GAN $_{T_1}$	<b>0.0702</b>	<b>26.5179</b>	<b>0.9162</b>
pGAN $_{T_2}$	0.2043	24.5725	0.8895
MI-GAN $_{T_2}$	<b>0.1814</b>	<b>25.9927</b>	<b>0.9194</b>

### B. $T_{2flair}$ Synthesis (MISO)

In this second set of experiments we train our MM-GAN model to synthesize  $T_{2flair}$  sequence in the presence of a varied number of input sequences (one, two or three). Contrasting from the MI-GAN models, this model is trained to generalize on number of different scenarios depending on the available input sequences. In this case, the number of valid scenarios are 7. We perform validation on the ISLES2015 dataset in order to directly compare with REPLICA [22] and MM-Synthesis [5]. The quantitative results are given in Table II. We note that the proposed MM-GAN ( $0.2262 \pm 0.0468$ ) clearly outperforms REPLICA’s unimodal synthesis models ( $0.271 \pm 0.10$ ) in all scenarios, as well as MM-Synthesis ( $0.236 \pm 0.08$ ) in majority

(4/7) scenarios. Our method also demonstrates an overall lower MSE standard deviation throughout testing (ranging between [0.03, 0.07], compared to REPLICA [0.08, 0.16] and MM-Synthesis [0.02, 0.13]) in all scenarios but one ( $T_2$  missing). The qualitative results for ISLES2015 are shown in Figure 2. Compared to MM-Synthesis (from qualitative results shown in their original paper [5]), our results are objectively sharper, with lower blurring artifacts. MM-GAN also preserves high frequency details of the synthesized sequence, while MM-Synthesis and REPLICA seem to miss most of these details. Qualitatively from Figure 2, MM-GAN follows the intensity distribution of the real  $T_{2flair}$  sequence in its synthesized version of  $T_{2flair}$ .

We found that using CL based learning did not help in MISO experiments, as the presence of more sequences does not necessarily increase the amount of information available. For example, the presence of both  $T_1$  and  $T_2$  does not result in better  $T_{2flair}$  synthesis (MSE=0.2541) compared to the presence of DW alone (MSE=0.2109). This is because, for every missing sequence, there tends to be some “highly informative” sequences that, if absent, reduces the synthesis performance by a larger margin. On the other hand, the presence of these highly informative sequences can dramatically boost performance, even in cases where no other sequence is present. Due to this, the assumption that leveraging a higher number of present sequences implies an easier case (i.e. more accurate synthesis) does not hold, and thus it becomes problematic to rank scenarios based on how easy they are, which renders CL useless in this case. Globally (for all valid scenarios, presented in next subsection), however, this assumption tends to hold due to the complex nature of interactions between sequences. CL helps tremendously in achieving a stable training of the network in the subsequent experiments (MIMO). For MISO, every scenario was shown to the network with uniform probability, throughout training.

TABLE II  
COMPARISON WITH UNIMODAL METHOD REPLICA AND MULTIMODAL METHOD MM-SYNTHESIS. THE REPORTED VALUES ARE MEAN SQUARED ERROR (MSE). BOLDFACE VALUES REPRESENT LOWEST VALUES OF THE THREE METHODS FOR A PARTICULAR SCENARIO.

Scenarios $T_1$ $T_2$ DW	REPLICA	MM-Synthesis	MM-GAN (Proposed)
- - ✓	0.278 (0.09)	0.285 (0.13)	<b>0.2109 (0.0575)</b>
- ✓ -	0.374 (0.16)	0.321 (0.12)	<b>0.2799 (0.0550)</b>
- ✓ ✓	0.235 (0.08)	0.214 (0.09)	<b>0.1826 (0.0332)</b>
✓ - -	0.301 (0.11)	<b>0.249 (0.09)</b>	0.2813 (0.0711)
✓ - ✓	0.225 (0.08)	0.198 (0.02)	<b>0.1918 (0.0392)</b>
✓ ✓ -	0.271 (0.12)	<b>0.214 (0.08)</b>	0.2541 (0.0661)
✓ ✓ ✓	0.210 (0.08)	<b>0.171 (0.06)</b>	0.1828 (0.0412)
<b>Mean</b>	0.271 (0.10)	0.236 (0.08)	<b>0.2262 (0.0468)</b>

### C. Multimodal Synthesis (MIMO)

We present results for our experiments on BRaTS2018’s HGG and LGG cohorts in Table III. In this experiment we train our proposed MM-GAN model on all 14 valid scenarios, in order to synthesize any missing sequence from any number or combination of available sequences. We observe that the



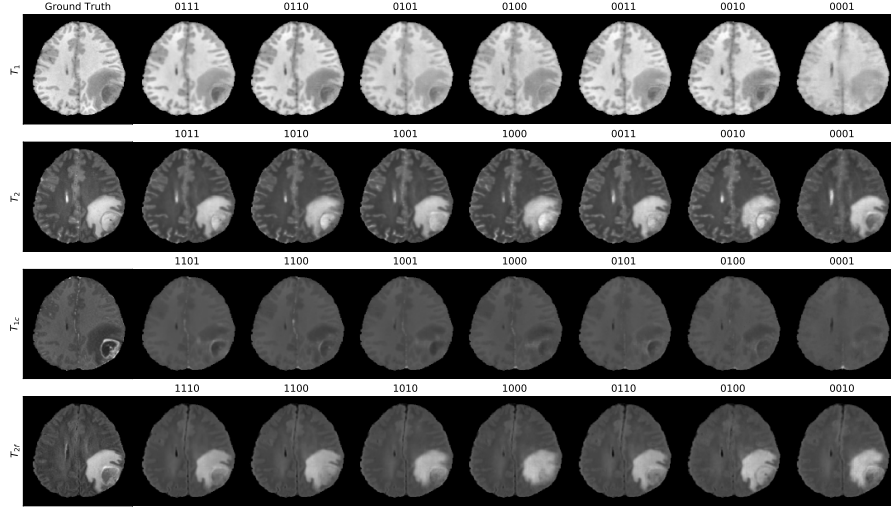


Fig. 3. Qualitative results from multimodal synthesis experiments with BRATS2018 dataset. Each row corresponds to a particular sequence, and shows the synthesized versions of that sequence in different scenarios. Note that a zero (0) represents missing sequence that was synthesized, and one (1) represents presence of sequence. The order of scenario bit-string is  $T_1$ ,  $T_2$ ,  $T_{1c}$ ,  $T_{2flair}$ . Patient images shown here are from *Brats18\_CBICA\_AAP\_1* from HGG cohort.

proposed MM-GAN model performs consistently well when synthesizing just one sequence, with high overall SSIM ( $>0.90$  in most cases except one in LGG), PSNR ( $>24.0\text{dB}$ ) values, and low MSE ( $<0.08$ ). As more sequences start missing, the task of synthesizing missing sequences gets harder. During the initial epochs of training, MM-GAN tends to learn the general global structure of the brain, without considering the local level details. This seems to be enough for the generator to fool the discriminator initially. However, as the training progresses and the discriminator becomes stronger, the generator is forced to learn the local features of the slice, which includes small details, especially the boundaries between the grey and white matter visible in the sequence. The qualitative results shown in Figure 3 show how MM-GAN effectively synthesizes the missing sequence in various scenarios, while preserving high frequency details that delineate between grey and white matter of the brain, as well as recreating the tumor region in the frontal lobe by combining information from available sequences. The synthesis of the tumor in the final images depend heavily on the available sequences. For example, the contrast sequence  $T_{1c}$  provides clear delineation of enhancing ring-like region around the necrotic mass, which is an important indicator of the size of the tumor. Presence of  $T_1$  and/or  $T_{2flair}$  sequence leads to improved synthesis of edema features. The contrast sequence  $T_{1c}$  provides unique information about the enhancing region around the tumor, which is usually not visible in any other sequence. Qualitatively, the  $T_2$  sequence does not seem to directly aid in synthesizing a particular region of tumor well, but coupled with other available sequences, it helps in better synthesis of tumor mass in the final synthesized slice (Figure 3).

As shown in Figure 4, we also observe that the method fills up lost details as can be seen in  $T_{2flair}$  sequence. The original ground truth sequence has the frontal lobe part cut off, probably due to patient movement or miss-registration. However MM-GAN recreates that part by using information

TABLE III  
EVALUATION ON BRATS2018 DATASET’S HIGH GRADE GLIOMA (HGG) AND LOW GRADE GLIOMA (LGG) COHORTS.

Scenarios				Dataset					
				HGG			LGG		
$T_1$	$T_2$	$T_{1c}$	$T_{2f}$	MSE	PSNR	SSIM	MSE	PSNR	SSIM
-	-	-	✓	0.0743	28.4552	0.9062	0.2534	24.1858	0.8401
-	-	✓	-	0.0862	27.5395	0.8982	0.1723	24.2399	0.8740
-	-	✓	✓	0.0632	28.9114	0.9175	0.1507	24.4712	0.8961
-	✓	-	-	0.0550	28.5015	0.9164	0.1735	24.9084	0.8837
-	✓	-	✓	0.0374	29.8410	0.9296	0.1612	25.8602	0.9048
-	✓	✓	-	0.0528	28.4044	0.9180	0.1202	25.3892	0.8861
-	✓	✓	✓	0.0311	29.4932	0.9265	0.0690	26.7615	0.9240
✓	-	-	-	0.0854	27.8242	0.9141	0.1664	26.2608	0.8952
✓	-	-	✓	0.0631	29.8457	0.9364	0.1508	26.7524	0.9264
✓	-	✓	-	0.0932	27.5185	0.9085	0.1854	23.5007	0.8759
✓	-	✓	✓	0.0848	29.1138	0.9304	0.1879	22.9748	0.9142
✓	✓	-	-	0.0517	28.9177	0.9242	0.1315	27.4112	0.8963
✓	✓	-	✓	0.0367	30.2639	0.9413	0.0963	30.5463	0.9488
✓	✓	✓	-	0.0633	27.5941	0.9093	0.1652	24.2623	0.8453
Mean				0.0658	28.5823	0.9172	0.1648	25.3607	0.8887

from the available sequences. An interesting side-effect of our approach is visible in  $T_{2flair}$  synthesis, where the synthesized versions of  $T_{2flair}$  exhibit higher quality details (Figure 4) than the original sequence, which was acquired in a very low resolution. This effect is the consequence of the method using high-resolution input sequences (all sequences except  $T_{2flair}$  are acquired at higher resolution) to synthesize the missing  $T_{2flair}$  sequence. This also suggests that our method may be used for improving or upscaling resolution of available sequences. However we do not investigate this further here, and leave it as future work.

We found that normalizing sequences with mean value is easier to train with, and naturally supports final layer activations like ReLU. We also investigated zero mean and



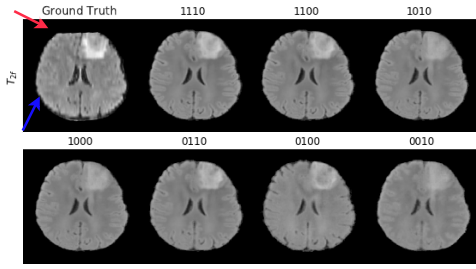


Fig. 4. Illustration of MM-GAN filling up parts in the scan that are originally missing in the ground truth. Red arrow shows the top part of brain that is missing, and is synthesized in all scenarios. Blue arrow highlights the high-frequency details that are missing in ground truth, but are synthesized in most images. The order of scenario bit-string is  $T_1$ ,  $T_2$ ,  $T_{1c}$ ,  $T_{2flair}$ . Patient images shown here are from *Brats18\_2013\_9\_1* from LGG cohort.

unit variance normalization and found that it under-performs relative to the mean normalization.

TABLE IV  
MM-GAN PERFORMANCE VARIATION WITH RESPECT TO NUMBER OF SEQUENCES MISSING FOR HGG AND LGG COHORT.

Dataset	Missing	MSE	PSNR	SSIM
HGG	1	$0.0539 \pm 0.0215$	$29.1162 \pm 0.9716$	$0.9268 \pm 0.0115$
	2	$0.0602 \pm 0.0170$	$28.9064 \pm 0.8095$	$0.9223 \pm 0.0090$
	3	$0.0752 \pm 0.0125$	$28.0801 \pm 0.4110$	$0.9087 \pm 0.0071$
LGG	1	$0.1296 \pm 0.0485$	$26.1362 \pm 2.8872$	$0.9080 \pm 0.0383$
	2	$0.1499 \pm 0.0208$	$25.5641 \pm 1.3161$	$0.8976 \pm 0.0157$
	3	$0.1914 \pm 0.0358$	$24.8987 \pm 0.8363$	$0.8732 \pm 0.0205$

We observe that the generators perform really well when they are constrained using a non-linear activation function at the final layer. However in the case of MISO, the limitation of the normalization type (dividing by mean value of sequence) used in MM-Synthesis prevents us from using a non-linear activation at the end of generator. This is due to the fact that some patients' data in SISS cohort from ISLES2015 contain negative intensity values, which after normalization stay negative. It can be seen that the MSE values reported in Table II tend to be higher than the ones reported in Table III, due to the latter set of experiments using ReLU activation at the end of generator.

We also observe that the proposed method shows graceful degradation as the number of sequences missing start increasing, which is apparent both qualitative and quantitatively in Figure 3 and Table IV. For instance, in HGG experiments, compared to having one sequence missing, the performance of MM-GAN drops on average by 11.6%, 0.7% and 0.4% in MSE, PSNR and SSIM respectively for scenarios where two sequences are missing. For scenarios where three sequences are missing, the performance drops on average by 39.5%, 3.5% and 1.9% in terms of MSE, PSNR and SSIM respectively compared to one sequence missing, and 24.9%, 2.8% and 1.4% when compared to scenarios where two sequences are missing. We observe that the method holds up well in generating sequences with high fidelity in terms of PSNR and SSIM even in harder scenarios where multiple sequences may be missing.

## VII. CONCLUSION

We propose a multi-modal generative adversarial network (MM-GAN) capable of synthesizing missing MR pulse sequences using combined information from the available sequences. Most approaches so far in this domain had been either unimodal, or partially multi-modal (multi-input, single-output). We present a truly multi-modal method that is multi-input and multi-output, generalizing to any combination of available and missing sequences. The synthesis process runs in a single forward pass of the network regardless of the number of sequences missing, and the run time is constant w.r.t number of missing sequences.

The first variant of our proposed MM-GAN, called MI-GAN outperformed the unimodal version pGAN in all three metrics (Table I). We also show that MM-GAN outperforms the best multimodal synthesis method REPLICa [22], as well as MM-Synthesis [5] in multi-input single-input synthesis of  $T_{2flair}$  sequence (Table II), and produces objectively sharper and more accurate results. In another set of experiments, we train our method on BraTS2018 dataset to set up a new benchmark in terms of MSE, PSNR and SSIM (Table III), and show qualitative results for the same (Figure 3). MM-GAN performance degrades as a function of number of missing sequences in Table IV but exhibits robustness in maintaining high PSNR and SSIM values even in harder scenarios. Finally, we show that our method is capable of filling in details missing from the original ground truth sequences, and also capable of improving quality of the synthesized sequences (Figure 4).

Although our approach qualitatively and quantitatively performs better than all other competing methods, we note that it has problems in synthesizing the enhancing subregion in  $T_{1c}$  sequence properly. This, however, is expected since  $T_{1c}$  sequence contains highly specific information about the enhancing region of the tumor that is not present in any other sequences. For future work, we note that the inherent design of our method is 2D, and an extension of the work which can take either 2.5D or 3D images into account may perform better both quantitatively and qualitatively.

## VIII. ACKNOWLEDGEMENTS

This work was partially supported by the NSERC-CREATE Bioinformatics 2018-2019 Scholarship. The authors would like to thank NVIDIA Corporation for donating a Titan X GPU. This research was enabled in part by support provided by WestGrid ([www.westgrid.ca](http://www.westgrid.ca)) and Compute Canada ([www.computecanada.ca](http://www.computecanada.ca)).

## REFERENCES

- [1] E. F. Jackson, L. E. Ginsberg, D. F. Schomer, and N. E. Leeds, "A review of MRI pulse sequences and techniques in neuroimaging," *Surgical Neurology*, vol. 47, no. 2, pp. 185–199, feb 1997.
- [2] C. Bowles *et al.*, "Pseudo-healthy image synthesis for white matter lesion segmentation," in *Simulation and Synthesis in Medical Imaging*. Springer International Publishing, oct 2016, pp. 87–96.
- [3] M. Havaei, N. Guizard, N. Chapados, and Y. Bengio, "HeMIS: Hetero-Modal Image Segmentation," in *Medical Image Computing and Computer-Assisted Intervention – MICCAI 2016*. Springer International Publishing, 2016, pp. 469–477.

- [4] T. Varsavsky *et al.*, “PIMMS: Permutation Invariant Multi-modal Segmentation,” in *Deep Learning in Medical Image Analysis and Multimodal Learning for Clinical Decision Support*. Springer International Publishing, 2018, pp. 201–209.
- [5] A. Chartsias, T. Joyce, M. V. Giuffrida, and S. A. Tsaftaris, “Multimodal MR Synthesis via Modality-Invariant Latent Representation,” *IEEE Transactions on Medical Imaging*, vol. 37, no. 3, pp. 803–814, mar 2018.
- [6] H. Chen *et al.*, “VoxResNet: Deep voxelwise residual networks for brain segmentation from 3D MR images,” *NeuroImage*, vol. 170, pp. 446–455, 2018.
- [7] S. Bakas *et al.*, “2017 International MICCAI BraTS Challenge,” 2017.
- [8] F. Isensee *et al.*, “Brain Tumor Segmentation and Radiomics Survival Prediction : Contribution to the BRATS 2017 Challenge,” in *Brainlesion: Glioma, Multiple Sclerosis, Stroke and Traumatic Brain Injuries*. Springer International Publishing, 2018, pp. 287–297.
- [9] G. Wang, W. Li, S. Ourselin, and T. Vercauteren, “Automatic brain tumor segmentation using cascaded anisotropic convolutional neural networks,” in *Brainlesion: Glioma, Multiple Sclerosis, Stroke and Traumatic Brain Injuries*. Springer International Publishing, 2018, pp. 178–190.
- [10] J. Dolz *et al.*, “HyperDense-Net: A hyper-densely connected CNN for multi-modal image segmentation,” *IEEE Transactions on Medical Imaging*, apr 2018.
- [11] S. Pereira, A. Pinto, V. Alves, and C. A. Silva, “Brain tumor segmentation using convolutional neural networks in MRI images,” *IEEE Transactions on Medical Imaging*, vol. 35, no. 5, pp. 1240–1251, 2016.
- [12] M. Havaei *et al.*, “Brain tumor segmentation with Deep Neural Networks,” *Medical Image Analysis*, vol. 35, pp. 18–31, jan 2017.
- [13] J. E. Iglesias *et al.*, “Is synthesizing MRI contrast useful for inter-modality analysis?” in *International Conference on Medical Image Computing and Computer-Assisted Intervention*. Springer, 2013, pp. 631–638.
- [14] D. H. Ye *et al.*, “Modality propagation: coherent synthesis of subject-specific scans with data-driven regularization,” in *International Conference on Medical Image Computing and Computer-Assisted Intervention*. Springer, 2013, pp. 606–613.
- [15] A. Jog, S. Roy, A. Carass, and J. L. Prince, “Magnetic resonance image synthesis through patch regression,” in *Proceedings - International Symposium on Biomedical Imaging*, vol. 2013. NIH Public Access, dec 2013, pp. 350–353.
- [16] A. Jog, A. Carass, D. L. Pham, and J. L. Prince, “Random forest FLAIR reconstruction from T1, T2, and Pd-weighted MRI,” in *Proceedings - International Symposium on Biomedical Imaging*. IEEE, 2014, pp. 1079–1082.
- [17] G. van Tulder and M. de Bruijne, “Why does synthesized data improve multi-sequence classification?” in *International Conference on Medical Image Computing and Computer-Assisted Intervention*. Springer, 2015, pp. 531–538.
- [18] A. Jog, A. Carass, D. L. Pham, and J. L. Prince, “Tree-encoded conditional random fields for image synthesis,” in *International Conference on Information Processing in Medical Imaging*. Springer, 2015, pp. 733–745.
- [19] S. Roy *et al.*, “Patch based synthesis of whole head MR images: Application to EPI distortion correction,” in *International Workshop on Simulation and Synthesis in Medical Imaging*. Springer, 2016, pp. 146–156.
- [20] Y. Huang, L. Beltrachini, L. Shao, and A. F. Frangi, “Geometry regularized joint dictionary learning for cross-modality image synthesis in magnetic resonance imaging,” in *International Workshop on Simulation and Synthesis in Medical Imaging*. Springer, 2016, pp. 118–126.
- [21] V. Sevettlidis, M. V. Giuffrida, and S. A. Tsaftaris, “Whole image synthesis using a deep encoder-decoder network,” in *International Workshop on Simulation and Synthesis in Medical Imaging*. Springer, 2016, pp. 127–137.
- [22] A. Jog *et al.*, “Random forest regression for magnetic resonance image synthesis,” *Medical Image Analysis*, vol. 35, pp. 475–488, jan 2017.
- [23] S. Olut, Y. H. Sahin, U. Demir, and G. Unal, “Generative adversarial training for MRA image synthesis using multi-contrast MRI,” in *International Workshop on Predictive Intelligence In Medicine*. Springer, 2018, pp. 147–154.
- [24] R. Mehta and T. Arbel, “RS-Net: Regression-Segmentation 3D CNN for Synthesis of Full Resolution Missing Brain MRI in the Presence of Tumours,” in *International Workshop on Simulation and Synthesis in Medical Imaging*. Springer, 2018, pp. 119–129.
- [25] M. Salem *et al.*, “Multiple Sclerosis Lesion Synthesis in MRI using an encoder-decoder U-NET,” *IEEE Access*, vol. 7, pp. 25 171–25 184, 2019.
- [26] B. Yu *et al.*, “Ea-GANs: Edge-aware Generative Adversarial Networks for Cross-modality MR Image Synthesis,” *IEEE Transactions on Medical Imaging*, pp. 1–1, 2019.
- [27] H. Van Nguyen, K. Zhou, and R. Vemulapalli, “Cross-domain synthesis of medical images using efficient location-sensitive deep network,” in *International Conference on Medical Image Computing and Computer-Assisted Intervention*. Springer, 2015, pp. 677–684.
- [28] S. Ul *et al.*, “Image Synthesis in Multi-Contrast MRI with Conditional Generative Adversarial Networks,” *IEEE Transactions on Medical Imaging*, pp. 1–1, 2019.
- [29] I. Goodfellow *et al.*, “Generative adversarial nets,” in *Advances in Neural Information Processing Systems*, 2014, pp. 2672–2680.
- [30] M. Mirza and S. Osindero, “Conditional generative adversarial nets,” *arXiv preprint arXiv:1411.1784*, 2014.
- [31] P. Isola, J.-Y. Zhu, T. Zhou, and A. A. Efros, “Image-to-image translation with conditional adversarial networks,” *The IEEE Conference on Computer Vision and Pattern Recognition (CVPR)*, pp. 1125–1134, 2017.
- [32] S. Reed *et al.*, “Generative adversarial text to image synthesis,” *Proceedings of The 33rd International Conference on Machine Learning*, pp. 1060–1069, 2016.
- [33] L.-C. Yang, S.-Y. Chou, and Y.-H. Yang, “MidiNet: A convolutional generative adversarial network for symbolic-domain music generation,” *arXiv preprint arXiv:1703.10847*, 2017.
- [34] J. Gauthier, “Conditional generative adversarial nets for convolutional face generation,” *Class Project for Stanford CS231N: Convolutional Neural Networks for Visual Recognition, Winter semester*, vol. 2014, no. 5, p. 2, 2014.
- [35] D. Ulyanov, A. Vedaldi, and V. Lempitsky, “Instance normalization: The missing ingredient for fast stylization,” *arXiv preprint arXiv:1607.08022*, 2016.
- [36] M. Mathieu, C. Couprie, and Y. LeCun, “Deep multi-scale video prediction beyond mean square error,” *arXiv preprint arXiv:1511.05440*, 2015.
- [37] L. Karacan, Z. Akata, A. Erdem, and E. Erdem, “Learning to generate images of outdoor scenes from attributes and semantic layouts,” *arXiv preprint arXiv:1612.00215*, 2016.
- [38] S. Kazemini *et al.*, “GANs for medical image analysis,” *arXiv preprint arXiv:1809.06222*, 2018.
- [39] P. Moeskops *et al.*, “Adversarial Training and Dilated Convolutions for Brain MRI Segmentation,” in *Deep Learning in Medical Image Analysis and Multimodal Learning for Clinical Decision Support*. Springer International Publishing, 2017, pp. 56–64.
- [40] Y. Xue *et al.*, “SegAN: Adversarial network with multi-scale L1 loss for medical image segmentation,” *Neuroinformatics*, vol. 16, no. 3–4, pp. 383–392, 2018.
- [41] S. Izadi, Z. Mirikharaji, J. Kawahara, and G. Hamarneh, “Generative adversarial networks to segment skin lesions,” in *2018 IEEE 15th International Symposium on Biomedical Imaging (ISBI 2018)*. IEEE, 2018, pp. 881–884.
- [42] A. Bentaieb and G. Hamarneh, “Adversarial Stain Transfer for Histopathology Image Analysis,” *IEEE Transactions on Medical Imaging*, vol. 37, no. 3, pp. 792–802, mar 2018.
- [43] C. Tanner *et al.*, “Generative adversarial networks for MR-CT deformable image registration,” *arXiv preprint arXiv:1807.07349*, 2018.
- [44] O. Ronneberger, P. Fischer, and T. Brox, “U-Net: Convolutional Networks for Biomedical Image Segmentation,” in *International Conference on Medical Image Computing and Computer-Assisted Intervention*. Springer, may 2015, pp. 234–241.
- [45] Y. Bengio, J. Louradour, R. Collobert, and J. Weston, “Curriculum learning,” in *Proceedings of the 26th Annual International Conference on Machine Learning*. ACM, 2009, pp. 41–48.
- [46] D. P. Kingma and J. Ba, “Adam: A method for stochastic optimization,” *arXiv preprint arXiv:1412.6980*, 2014.